Università degli Studi di Padova
Dipartimento di Fisica ed Astronomia "G. Galilei"

Master's Degree Thesis in physics of matter

Synthesis and characterization of dye-doped polymeric thin films to be used as gain medium in plasmonic nanolasers

Master Candidate:
MOHAMMAD MOHSENI FAZEL

Supervisor:
Prof. Tiziana Cesca

Academic Year 2022/2023

Dedicated to my loving family, whose unwavering support and encouragement have been my guiding light throughout this academic journey

Abstract

In the search for highly efficient and miniaturized light sources, plasmonic nanolasers have proven to be promising candidates for applications in the fields of telecommunications, sensor technology and medical diagnostics. The core element that determines the performance of these nanolasers is the gain medium that enables light amplification and emission. This thesis focuses on the synthesis and comprehensive characterization of dye-doped polymeric thin films engineered to serve as a tailored gain medium within plasmonic nanolasers.

The purpose of this Master thesis is the complicated process of material synthesis, which involves the careful selection of polymer matrices and laser dyes and culminates in the production of thin films with precise control over thickness and homogeneity. Experimental investigations focus on the optical and morphological properties of these films, including absorption and emission spectra, photoluminescence behaviour and detailed analysis of surface morphology

The sample comprises gold nanodisks organized in a two-dimensional square pattern with an interspacing of 600 nm. Initially, its structure was examined using imaging methods like Atomic Force Microscopy and Scanning Electron Microscopy. Then the absorbance and the emission spectra of the solutions with different concentration of dye(IR140) and PMMA were measured. Subsequently, a liquid solution of IR-140 dissolved in PMMA was layered onto the nanoarray. Utilizing finite-elements simulations through COMSOL Multiphysics, an investigation the thickness for different concentration of the dye, was conducted.

Contents

Abstract **iii**

Introduction **1**

1 Plasmonic Nanolasers **3**
1.1 Working Principle . . . 3
1.2 Laser Beam Characteristics . . . 6
1.3 Plasmonic Nanolasers . . . 8
1.3.1 Surface Plasmon Resonances . . . 8
1.4 Plasmonic nanoparticle arrays . . . 9
1.4.1 The gain medium . . . 11

2 Sample synthesis and characterization **15**
2.1 Creating the polymer film . . . 15
2.1.1 Spin coating method . . . 16
2.1.2 Making the samples . . . 17

3 Experimental **19**
3.1 Gold Nanostructured Arrays . . . 19
3.2 Morphological Characterization . . . 19
3.2.1 Atomic Force Microscopy (AFM) . . . 20
3.2.2 Scanning Electron Microscopy(SEM) . . . 22
3.2.3 SEM images . . . 24
3.3 Lasing Emission Setup . . . 24
3.4 Characterization of the emitter . . . 26
3.4.1 Absorbance measurments . . . 26
3.4.2 Fluorescence measurments . . . 27

4 Results and Discussion **31**
4.1 Dye-doped polymer film . . . 31
4.1.1 Sample prepration . . . 31
4.1.2 Thickness measurement with AFM . . . 31
4.2 Absorbance measurement of the dye-doped . . . 33

4.3 Emission Measurement with Fluoromax 35
4.3.1 Thickness analysis 37

5 Conclusions **39**

Bibliography **40**

List of Figures **44**

List of Tables **44**

Introduction

In the dynamic field of photonics and nanotechnology, the emergence of high-power plasmonic nanolasers has ushered in a new era with far-reaching implications for various fields, ranging from telecommunications to advanced sensing and diagnostic applications in the medical field. The linchpin of these breakthrough nanolasers is the gain medium, an instrumental component responsible for the amplification and emission of light.

In recent years, numerous research groups have dedicated their efforts to the exploration of plasmonic nanolasers. The state of the art about these devices involves groups as that of T. Odom at the University of Northwestern in Illinois, or B. Cunningham at the University of Illinois, who independently use different nanostructures coupled to liquid gain media[1][2][3][4]. Also the group of A. F. Koenderink, at AMOLF in Amsterdam, is studying this kind of system, investigating the role of the nanoparticle order[5].

The concept of nanolasers involves replacing conventional, macroscopic optical cavities with open cavities created, for example, by nanostructuring. The lack of a standard cavity in these devices makes it possible to bypass the diffraction limit and thus produce miniaturized laser sources. This achievement is due in part to the significant advances that have been made in nanofabrication techniques in recent years. The compact size of nanolasers offers various potential applications, such as optical interconnections, the study of biological systems, and their use in near-field spectroscopy and sensing[6].

This thesis embarks on a comprehensive exploration into the intricate universe of plasmonic nanolasers, with a particular emphasis on the synthesis and in-depth characterization of dye-doped polymeric thin films. The selection of the gain medium within plasmonic nanolasers holds paramount significance, as it fundamentally dictates the optical attributes and the overall performance of these photonics devices. Dye-doped polymeric thin films, a compelling and versatile choice, exhibit the unique characteristics of tunability, simplicity in fabrication, and seamless integration with plasmonic nanostructures.

The central aim of this research endeavor is to unravel the intricate process of synthesizing these polymeric thin films, encompassing a diverse range of dye dopants, and embarking on a comprehensive exploration of their optical properties. Through a systematic and rigorous approach to experimentation and in-depth analysis, we seek to gain profound insights into the behaviors and capabilities of these materials, particularly their suitability as high-performance gain media in the context of plasmonic nanolasers.

Subsequent chapters will provide a detailed expedition through the methodologies em-

ployed in the synthesis process, the sophisticated experimental techniques harnessed for thorough characterization, and, finally, the unveiling of the results from our meticulous investigations.

Chapter 1

Plasmonic Nanolasers

1.1 Working Principle

The term LASER, which stands for light amplification by stimulated emission of radiation, refers to a light source whose emitted radiation is distinguished from other light sources by a high degree of spatial and temporal coherence, high monochromaticity, directionality, and high brilliance. The first theoretical foundation of LASER was given by Einstein in 1917 with his studies on spontaneous and stimulated emission of electromagnetic radiation[7].

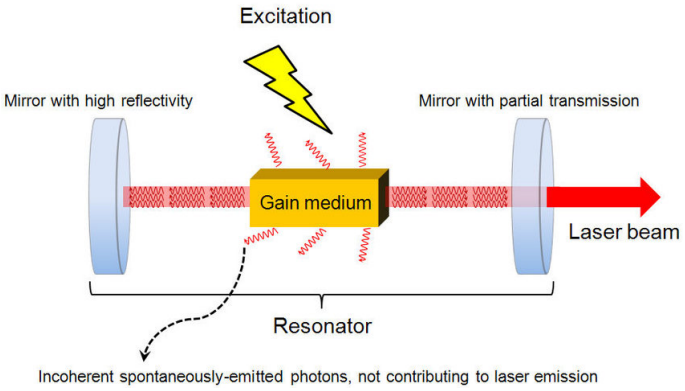

Figure 1.1: Laser cavity composed of a gain medium between two reflective mirrors

Every laser system primarily consists of an energy source to pump the active medium which is sandwiched between two optically parallel, highly reflecting mirrors with one of them partially transmitting as shown in Fig 1.1 . Pumping can be electrical or optical, and the gain medium can be solid, liquid, or gas. It has the ability to amplify the light beam traveling through it by stimulated emission. The gain medium is positioned between a pair of mirrors in such a way that light oscillating between the mirrors passes through it many times achieving significant amplification[8].

In a specific quantum system (atom, molecule, or crystal), we consider two energy levels, 1 and 2, which have energies E1 and E2, respectively which shown in Fig1.2 . We'll assume for the sake of simplicity that level 1 represents the system's ground state, or the

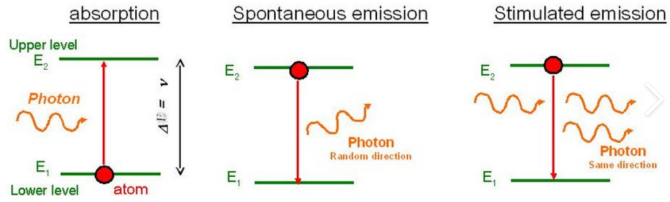

Figure 1.2: Energy diagram illustrating how absorption, stimulated emission, and spontaneous emission work.

state with the lowest allowed energy, and level 2 represents the system's first excited state. When this energy is released in the form of an electromagnetic (em) wave, the process is called spontaneous or radiative emission and corresponds to the emission of a photon with energy:

$$h\nu = E_2 - E_1 \tag{1.1}$$

where ν is the photon's frequency and h is the Planck constant. Radiative emission is only one of the system's possible decay mechanisms; there are other, non-radiative processes as well, in which case the energy difference between E2 and E1 is released in other ways, such as the kinetic or internal energy of the environment. Now let's have a look at the scenario once again where the system is in state 2 and is struck by a photon with frequency

$$v = \frac{E1 - E2}{h} \tag{1.2}$$

There is a finite probability that the wave causes the system to undergo the transition 2 to 1 by emitting a photon that adds to the incident one. The term for this process is stimulated emission. in the case of spontaneous emission the photon emitted during the transition can be emitted in any direction and does not have a clear phase relationship with the other photons released. For stimulated emission instead,Since the input electromagnetic wave (photon) forces the process, each photon is emitted in phase with the incident wave and in the same direction. Let's finally think about the absorption process, which always occurs between levels 1 and 2 The system, which is initially in the fundamental state 1, absorbs an incident photon of frequency v, which corresponds to the energy difference between two states, making a transition to the excited level 2.

In a laser, the population inversion refers to the situation where more atoms or molecules in an active medium are in an excited state than in the ground state. This is in contrast to the condition found in thermal equilibrium where most atoms are in the ground state.

How is it feasible to create a population inversion? The first suggestion might be to think about a two-level system that has a powerful enough em wave beaming on it at frequency ν. If N1 is initially grater than N2, stimulated emission is dominated by absorption. There will be more atoms promoted from level 1 to level 2 than vice versa. However, once the two populations are equal, the material becomes transparent to incident radiation, with the number of photons absorbed via unit of time being equal to the number of photons emitted per stimulated emission. Therefore, one cannot achieve population inversion

by employing a two-level system alone. Population inversion requires the consideration of three or more layers. the three-level and four-level systems' operational schemes. If the transition from level 3 to level 2 is swift enough, population inversion between levels 1 and 2 can be attained for the three-level plan. However, the system must reach the condition $N_1 > \frac{N_t}{2}$ which N_t is the total population in order to achieve the population inversion. Instead, for a four-level scheme, the ground level is identified as level 0, from which atoms are raised to level 3. From this level, the atoms rapidly decay into the level 2 and atoms in level 1 rapidly decay to level 0.This shows that a four-level laser is far more effective and feasible than a three-level laser since just a minimal number of atoms need to be excited in level 2 to create population inversion as shown in Fig 1.3. Theoretically, any system with more than two levels can be represented as a three- or four-level system.

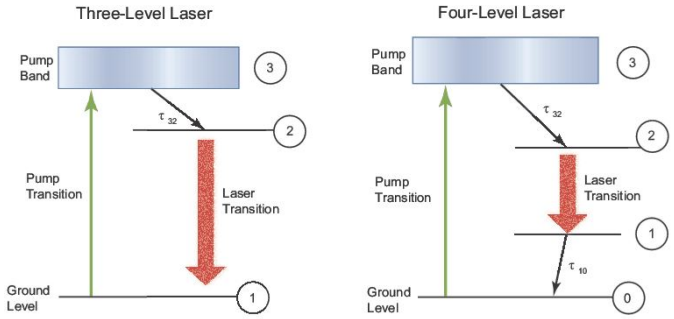

Figure 1.3: Three-level and four-level laser schemes

In a laser system with four energy levels, a set of rate equations can be formulated to describe the population dynamics within these levels. This configuration typically includes the ground state, which is the lowest energy level, the pump state responsible for energy absorption to achieve population inversion, the upper lasing state where laser emission originates, and another energy level, the lower lasing state, involved in the laser transition process. For a four-level system with non-degenerate levels we can write the system of rate equations as:

$$\frac{dN0(t)}{dt} = \frac{N1(t)}{\tau_{10}} + \frac{N3(t)}{\tau_{30}} - W_p N0(t) \tag{1.3}$$

$$\frac{dN1(t)}{dt} = \frac{N2(t)}{\tau_{21}} + \frac{N1(t)}{\tau_{10}} - F\sigma_{21}[N1(t) - N2(t)] \tag{1.4}$$

$$\frac{dN2(t)}{dt} = \frac{N3(t)}{\tau_{32}} + \frac{N2(t)}{\tau_{21}} + F\sigma_{21}[N1(t) - N2(t)] \tag{1.5}$$

$$\frac{dN3(t)}{dt} = -\frac{N3(t)}{\tau_{32}} - \frac{N3(t)}{\tau_{30}} + W_p N0(t) \tag{1.6}$$

where N_p is the rate of the pumping process, and τ expresses the characteristic times of the various decays. It should be noted that in order to achieve lasing, 32 and 10 decays must be fast. This translates into requiring τ_{32} and τ_{10} to be smaller than the characteristic time of the 21 lasing transition.

These rate equations describe the interactions between atoms in different energy levels and the incident radiation in a four-level laser system. They are fundamental in understanding the behavior of laser systems, including achieving and maintaining population inversion and lasing action.

A conventional laser consists of a resonant cavity containing a gain medium. Photons travel inside the cavity and at any trip they are able to produce more photons due to stimulated emission.

Cavities offer several advantages in laser systems. For instance, the presence of a cavity restricts the lasing frequency or wavelength to specific values, allowing the formation of as longitudinal modes. The wavelength selection results in a narrower emission peak compared to the peak width of the gain medium, leading to increased coherence of the emitted radiation. Additionally, the use of a cavity enhances photon confinement within the system, particularly within longitudinal modes, which promotes more efficient stimulated emission and the buildup of laser emission.

An important parameter in describing a cavity is the quality factor (Q), which quantifies the duration that photons remain within the cavity. Considering mirror reflectivities and losses, the photon lifetime within a cavity of length L can be expressed as

$$\tau_{\text{cav}} = \frac{L}{c\gamma} \tag{1.7}$$

where γ are the logarithmic cavity losses.

The quality factor (Q) can be expressed as the result of 2π times the energy stored divided by the energy lost within a single oscillation cycle. Using this definition, a connection between the quality factor and the photon lifetime of the cavity can be derived as follows:

$$Q = 2\pi\nu\tau_{\text{cav}} \tag{1.8}$$

Furthermore, one can establish a relationship between the quality factor and the emission peak width as:

$$Q = \frac{\nu}{\Delta\nu_{\text{cav}}} \tag{1.9}$$

This relation implies that a high quality factor results in a narrow emission peak.

Where

$$\Delta\nu_{\text{cav}} = \frac{1}{2\pi\tau_{cav}} \tag{1.10}$$

is the bandwidth of the mode at frequency ν.

1.2 Laser Beam Characteristics

Coherence

Temporal coherence: Consider the electric field in a generic point P of the wavefront of an em wave at time t and time $(t+\tau)$. If the difference of phase between $E(t)$ and $E(t+\tau)$

remains constant for any time $0 \leq \tau \leq \tau_0$, the electromagnetic wave has partial temporal coherence with a coherence time equal to τ_0 ; if the phase difference remains constant for any one value of τ, it is said that the em wave has perfect temporal coherence. It is worth noting that the two concepts of spatial and temporal coherence are distinct and that, for example, an em wave can have partial temporal coherence while being perfectly coherent from the spatial point of view.

Spatial coherence: Given the definition of wavefront, the phase difference between the two electric fields at time t_0 will be zero given two points P_1 and P_2 on the wavefront of an em wave. The two points will be coherent if this phase difference remains zero at any time t, and if this occurs, regardless of where the two spots on the wavefront are, it is said that the em wave has complete spatial coherence.

Directionality

We shall give special focus to directionality for our samples because it is a crucial quality that is used extensively in many laser applications. This characteristic results from the active material being positioned in an open resonant cavity. In a Fabry-Perot cavity, for example, only a resonant mode can oscillate. However, due to the resonator's design, an em wave with a proper frequency and travelling orthogonally to the mirrors can oscillate[9].

Short pulse duration

Pulsed emission can be produced using a variety of methods, including Q-switching and mode locking. It is not an inherent property of laser beams. Due to its ability to reach high pulse energies or high peak pulse powers, pulsed lasers are widely used in a variety of applications. By providing a loss mechanism that surpasses the gain of the medium, the Q-switching technique enables the generation of ns pulses. Once energy in the medium has nearly reached its maximum storage capacity, it is quickly removed, creating brief pulses of peak power and high energy. The mode locking technique, on the other hand, enables the creation of light pulses with durations that are about equivalent to the inverse of the line width of the laser transition.

Brightness

Brightness is defined as the amount of energy emitted by an electromagnetic wave source per unit surface area per unit solid angle.

Brightness B for an isotropic source is a constant. Since a laser beam is collimated, B for a laser beam can be very high.

Given a beam with power P, diameter D and divergence of θ, assuming that θ is very small (i.e., $\cos\theta \approx 1$).

$$B = \frac{4P}{(\pi D\theta)^2} \tag{1.11}$$

1.3 Plasmonic Nanolasers

1.3.1 Surface Plasmon Resonances

Plasmons are the result of the coordinated motion of free electrons in materials like metals or semiconductors when subjected to external electromagnetic fields, particularly at optical frequencies. They represent a kind of "quasiparticle," originating from the collective behavior of many electrons in a material.

Plasmons enable the confinement and manipulation of electromagnetic energy on a nanoscale level, playing a pivotal role in the domain of nanophotonics. They are instrumental in the development of various optical technologies, such as plasmonic sensors, nanoantennas, and plasmonic waveguides. Furthermore, plasmonic effects serve as the foundation for phenomena such as surface-enhanced Raman scattering (SERS) and increased interactions between light and materials. These effects have practical applications in various fields, including sensing, imaging, and energy harvesting.

The progression of plasmonic nanolasers represents a storyline that spans numerous decades of scientific exploration and technological progress. This comprehensive historical overview illuminates the gradual growth and noteworthy achievements in this area, offering crucial background for the research conducted in this thesis.

The inception of plasmonic nanolasers can be traced back to the intersection of two pivotal domains: plasmonics and laser physics. Plasmonics, became increasingly influential in the latter half of the 20th century. These collective electron oscillations at the interface of materials such as metals promised to offer new ways to manipulate and control light. In parallel, the field of laser physics was experiencing rapid growth, with the advent of lasers and their versatile applications in diverse industries.

The emergence of plasmonic nanolasers as a distinct research area can be largely attributed to advancements in nanotechnology. The ability to engineer and manipulate materials at the nanoscale opened doors to unprecedented possibilities. Researchers sought to harness the unique properties of surface plasmons to create ultra-compact lasers capable of confining light to dimensions smaller than the wavelength of light itself. One of the fundamental breakthroughs was the development of metal-clad microcavity lasers, which could efficiently guide and manipulate plasmonic modes. This was a turning point, as it paved the way for the design and realization of plasmonic nanolasers. The intricate interplay between plasmon resonances and the gain medium within these structures allowed for the development of nanoscale light sources with an array of applications.

Plasmonic nanolasers have since found their place in fields such as on-chip photonics, ultra-fast data transmission, biological and chemical sensing, and quantum optics. Their versatility and ability to operate on a scale inconceivable a few decades ago make them indispensable tools for researchers and engineers.

When we work with metal nanoparticles (with lateral dimensions smaller than the incident wavelength) enveloped by a dielectric material, the modes that can be triggered are termed Localized Surface Plasmons. The electric field is confined within the particle

itself and extends to a range of a few tens of nanometers from their surface. This phenomenon enables the shrinking of laser dimensions, overcoming the limitations imposed by diffraction.

Localized Surface Plasmon Resonances(LSPR) refers to a collective oscillation of free electrons within noble metal nanoparticles, resulting from the interaction between incident electromagnetic radiation and the nanostructure's surface as shown in Fig 1.4. This resonance phenomenon occurs at specific wavelengths and leads to enhanced local electromagnetic fields, making LSPs a fundamental concept in the field of nanophotonics.

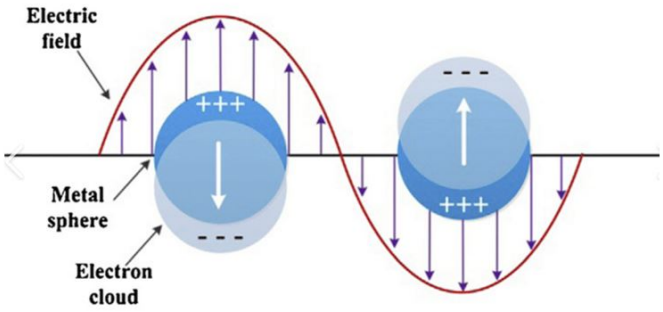

Figure 1.4: A diagram showing the collective oscillation of electrons in a metal under electric field

The characteristics of LSPR are contingent on various factors, including the size, shape, electron density, effective mass of the nanostructures, and the dielectric properties of the surrounding medium[10].

1.4 Plasmonic nanoparticle arrays

Surface Lattice Resonance (SLR) emerges as a fascinating and crucial phenomenon within the domain of nanophotonics, offering a multitude of opportunities and a means to revolutionize the interaction between light and nanostructures.

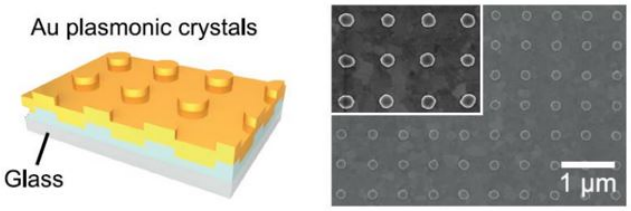

Figure 1.5: periodic nanoscale structure on surface

Fundamentally, SLR originates from the regular positioning of nanosized structures on surfaces. These structures, whether they are plasmonic nanoparticles, dielectric resonators,

or other nanoantennas, are meticulously arranged to form a lattice. When they interact with incoming light, this configuration triggers resonant effects that profoundly impact the optical behavior of the system[11].

Placing plasmonic nanostructures in a well-organized configuration can activate collective plasmonic modes that are mediated by the lattice. Dipolar interactions result in the creation of a new narrow linewidth plasmonic resonance, close to the diffraction order of the lattice. A plasmonic system based on these collective resonances is one potential method to reduce losses since the interaction of plasmonic nanoparticles with these collective extended modes suppresses radiative damping, which is the primary contributor to the plasmon resonance linewidth.

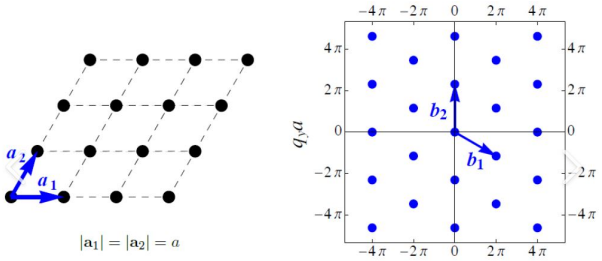

Figure 1.6: Triangular lattice in real space(left) and Reciprocal lattice(right)

The form, size, and composition of nanoparticles, as well as the environment and the polarization of the incident radiation, all have an impact on the properties of SLRs. SLRs also heavily depend on the interparticle distance and the long-range order in the lattice due to their collective behavior[12] . Plasmonic nanolasers have shown interesting properties, such as directional emission and spatial coherence. The size of the array was shown to be in determining the lasing threshold and population inversion dynamics. Plasmonic nanoarrays were also used to achieve real-time tunable lasing[13].

The plasmonic properties of arrays of metal nanoparticles (NPs) come into play when these NPs are arranged in a periodic array with the spacing being approximately equal to the wavelength of the plasmon resonance. In this scenario, the plasmons in the NPs couple with the diffractive orders of the array, giving rise to a distinct and narrow resonance peak known as Surface Lattice Resonance (SLR). What sets SLR apart is that its extinction peak is both higher and narrower compared to the Localized Surface Plasmon Resonance (LSPR) peak. This makes SLR exceptionally efficient and suitable for various applications like sensing and lasing. From an analytical perspective, these effects can be explained by considering changes in polarization due to interactions among particles in an array, rather than single particles.

We will go over how a plasmonic array, in this case a two-dimensional array of metallic nanostructures, can take the place of an optical cavity to create a plasmonic nanolaser, moving laser technology closer to being smaller than the diffraction limit[14] .

Surface Plasmon Polaritons (SPP) and Localized surface Plasmons (LSP) are used in plasmonic nanolasers to compress light into spaces smaller than the wavelength. As we

saw, the LSPRs enable nanoparticles to localize the EM field three-dimensionally within tens of nanometers of their surface. Instead of producing photons, a gain medium nearby the excited nanoparticles via the pump process might transfer energy to the LSPR of the nanoparticles in a non-radiative manner. The SPs already present in the nanosystem promote these transitions, and because this non-radiative energy transfer is stimulated, a large number of coherent surface plasmons are produced in a single mode as shown in Fig 1.7 . In order to produce a laser emission, the energy stored in the plasmon oscillations can be reemitted[15].

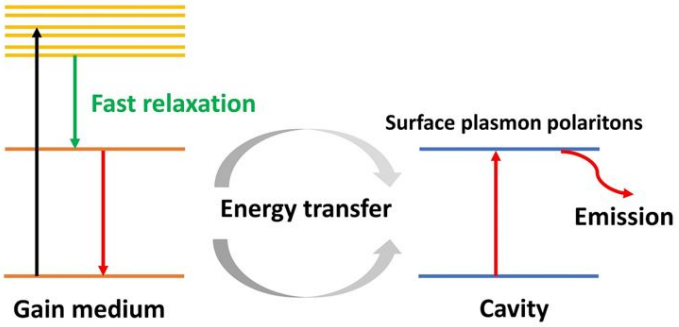

Figure 1.7: Schematic illustration of a plasmonic nanolaser

Additionally, due to the quick non-radiative decay of the plasmons, plasmonic nanolasers that use LSR or SPP as a cavity exhibit ultra-fast modulation on the femtosecond time scale.

Due to the constructive interference between the nearby nanoparticles, a plasmonic nanolaser can allow effective outcoupling and directional lasing emission when nanostructures acting as resonant cavities are arranged in a periodic pattern [19]. Each nanocavity oscillates in phase under the control of the lattice modes, producing a high-quality cavity mode for coupling the near-field energy into free space[12] .

This cavity mode can be connected to hybrid lattice plasmon modes that result from the coupling of individual nanoparticle LSPs to periodic array diffraction modes. At room temperature, this mode can suppress radiative loss and offer visual feedback for directional laser output. These lattice plasmonic resonances (SLRs), as previously stated, are supported by metallic nanoparticles arranged in a periodic array in a medium with a uniform refractive index, and their characteristics are influenced by the individual LSPRs of each nanoparticle, the lattice parameters, and the surroundings.

1.4.1 The gain medium

The gain medium typically dye molecules in a liquid solution or solid matrix is layered on top of an array of metal NPs in these devices. The gain layer's refractive index is often selected to be as close to the substrate's refractive index as is practical.

The surface plasmons at the NPs' surface, which result in a significant field enhancement, provide light confinement. Surface Lattice Plasmons can also be excited since the

particles are arranged in an ordered array and the surrounding environment's refractive index is almost uniform.

The metal NPs enable nonradiative energy transfer to the lattice plasmons due to their existence. After the initial excitations, the presence of earlier plasmons stimulates the process, leading to the coherent generation of a significant number of surface plasmons.Lasing emission results from the coherent reemission of the energy that was previously stored in the plasmon. Additionally, because NPs are organized in an ordered array, constructive interference in the fields created by nearby particles allows lasing emission to have a high degree of directionality.

Bleaching is a specific occurrence that takes place when dye molecules are present. It alludes to a change made to the chemical structure that stops molecules from getting stimulated. Bleaching consequently results in a lower quantum yield. The presence of contaminants or the chemical characteristics of the substance in which the gain molecules are dissolved or embedded can both contribute to bleaching. Additionally, photochemical processes could take place and change the molecular structure of molecules exposed to a high photon flux, leading to bleaching. Since gain molecules are activated by a high-fluence beam, a phenomena termed as photobleaching must be taken into account for our purposes.

The quantum yield (η) is a significant parameter in the context of organic dyes. It is defined as the ratio of the number of emitted photons to the number of absorbed photons, expressed as:

$$\eta = \frac{\text{number of emitted photons}}{\text{number of absorbed photons}} = \frac{\tau_t}{\tau_r} \tag{1.12}$$

where τ_r is the radiative lifetime, and τ_t can be determined from the reciprocal sum of the possible decay lifetimes:

$$\tau_t = \frac{1}{\sum_i \left(\frac{1}{\tau_i}\right)} \tag{1.13}$$

Let us consider the coupling between a plasmonic NP and gain molecules as a last observation. The field enhancement provided by the plasmon resonance is projected to result in a rise in the fluorescence rate for emitters closer to the NP. The fluorescence rate, however, reduces if molecules are too close to the particle. An rise in the nonradiative decay rate is what causes the phenomena known as quenching. Forster Resonant Energy Transfer (FRET), a process in which energy transfer happens between donor molecules and a metal surface, is the cause of the nonradiative decay rate intensifying.

The most intriguing method for solving this innovative challenge, which involves lasing emission based on plasmonic interaction, was put out by Dridi and Schatz in 2013. It uses Maxwell's equation for the em field and rate equations for the gain medium.

In this classical approach, the energy-transfer rate between the em field and the gain medium molecules is

$$\frac{dU_{ij}(t)}{dt} = E(t) \cdot \frac{dP_{ij}(t)}{dt} = \frac{dN_i(t)}{dt} \cdot \omega_{ij} \tag{1.14}$$

that is equal to the transition rate per photon energy.

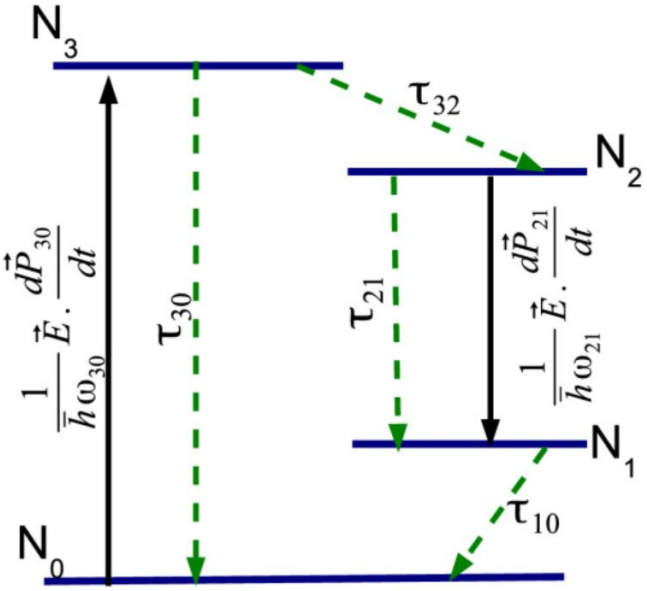

Figure 1.8: Four-level model used to describe the dye molecule

Taking into account a four-level system[16] as shown in Fig 1.8 to describe the energy state of gain medium,the system of rate equations can be written as:

$$\frac{dN0(t)}{dt} = \frac{N1(t)}{\tau_{10}} + \frac{N3(t)}{\tau_{30}} - \frac{1}{\hbar\omega} E_1(t) N0(t) \frac{dP30(t)}{dt} \tag{1.15}$$

$$\frac{dN1(t)}{dt} = \frac{N2(t)}{\tau_{21}} - \frac{N1(t)}{\tau_{10}} - \frac{1}{\hbar\omega_{21}} E_1(t) N0(t) \frac{dP21(t)}{dt} \tag{1.16}$$

$$\frac{dN2(t)}{dt} = \frac{N3(t)}{\tau_{32}} + \frac{N2(t)}{\tau_{21}} + \frac{1}{\hbar\omega_{21}} E_1(t) N0(t) \frac{dP21(t)}{dt} \tag{1.17}$$

$$\frac{dN3(t)}{dt} = -\frac{N3(t)}{\tau_{32}} - \frac{N3(t)}{\tau_{30}} + \frac{1}{\hbar\omega} E_1(t) N0(t) \frac{dP30(t)}{dt} \tag{1.18}$$

The electric field E(t) represents the overall electric field, which is the sum of the contributions from molecules' radiation emissions, incident radiation, and the electric field produced by nanostructures.

Chapter 2

Sample synthesis and characterization

2.1 Creating the polymer film

The method for creating polymer films typically involves several techniques, including spin coating, dip coating, and layer-by-layer assembly[17]. The initial step is the selection of an appropriate polymer material for the film. The choice of polymer depends on the specific characteristics desired for the film, such as transparency, flexibility, or electrical conductivity. Once the polymer is chosen, it is often dissolved in a suitable solvent to create a solution. The choice of solvent is a critical factor as it can impact various properties of the film, including its thickness and uniformity. Additionally, the concentration of the polymer in the solution plays a crucial role.

After the solution is prepared, the next step is to prepare the substrate, which is the surface on which the polymer film will be deposited. Substrates can be made of materials like glass, silicon, or other substances, depending on the intended application. Proper cleaning and preparation of the substrate are essential to ensure good adhesion.

There are different techniques for depositing the polymer film, including spin coating, where a small amount of the polymer solution is dispensed onto the substrate and then spun at high speeds to create a thin and uniform film. Dip coating, on the other hand, involves immersing the substrate into the polymer solution and withdrawing it at a controlled speed, with the film's thickness determined by the withdrawal rate. Another method, known as layer-by-layer assembly, alternately deposits layers of oppositely charged polymers onto the substrate, resulting in a multilayer film.

Once the film is deposited, it undergoes characterization to ensure it meets the desired properties and thickness. Based on the results of this characterization, adjustments to the deposition process may be necessary. Parameters such as solution concentration, spin speed, or dipping rate can be fine-tuned to achieve the desired film properties.

2.1.1 Spin coating method

Spin coating is a widely employed method for creating thin and uniform films on substrates. It is particularly valuable in materials science for applications requiring precise control over film thickness and quality.

The fundamental principle behind spin coating involves the radial spreading of a solution or suspension on a rotating substrate. As the substrate rotates, centrifugal force drives the outward flow of the liquid. At the same time, solvent evaporation occurs, leaving behind a thin film on the substrate which shown in Fig 2.1 .

Several factors influence the film formation during spin coating, including the rotation speed (ω), solution concentration (C), viscosity (η), and solvent properties[18].

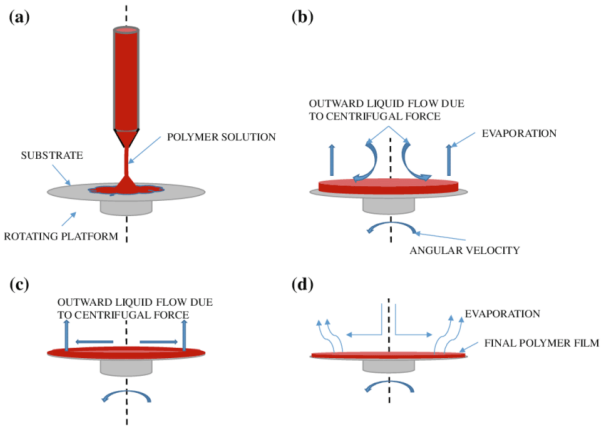

Figure 2.1: Spin coating process.(a)polymer solution add to the substrate on the rotating platform.(b)evaporation process and liquid flow goes outward due to the centrifugal force.(c)angular velocity in different steps and times.(d)final polymer film.

Solution Concentration (C): The solution concentration (C) refers to the amount of solute (substance being dissolved) present in a given volume of solvent (the dissolving medium). It is typically expressed in terms of mass per unit volume or moles per unit volume. The formula for solution concentration is as follows:

$$C = \frac{m}{V}$$

where C represents the solution concentration,m is the mass of the solute and V is the volume of the solvent.

Viscosity (η): Viscosity (η) is a measure of a fluid's resistance to flow. It quantifies the internal friction within a fluid as it moves. Viscosity is commonly described in terms of dynamic viscosity (η), which is the ratio of shear stress to shear rate. The formula for dynamic viscosity is as follows:

$$\eta = \frac{\text{Shear Stress}}{\text{Shear Rate}}$$

In more detail, it can be represented as:

$$\eta = \frac{F}{A \cdot \frac{dy}{dx}}$$

where, (η) represents the dynamic viscosity, F is the shear stress (force applied parallel to the surface), A is the area over which the force is applied and $\frac{dy}{dx}$ is the change in velocity (shear rate) with respect to the change in distance. These parameters are used to characterize a fluid's resistance to deformation and flow. The higher the viscosity, the more resistant the fluid is to flowing.

The film thickness (h) is a crucial parameter that can be described by the formula:

$$h = \frac{K}{\sqrt{\omega}} \tag{2.1}$$

Here, K represents a constant that depends on the solution properties and the solvent.

The spin coating process involves several key steps. Firstly, the choice of material is essential; the selected polymer or material should exhibit suitable solubility and viscosity properties. Secondly, a solution is prepared by dissolving the chosen material in a compatible solvent. The concentration of the material in the solution can be adjusted to control film thickness.

Substrate preparation is critical to ensure the substrate is clean and free from contaminants or particles that might affect film quality. The deposition process begins with dispensing a small amount of the solution onto the substrate's center, followed by placing the substrate on a spin coater chuck.

The spin parameters, including the rotation speed (ω), acceleration, and deceleration rates, are adjusted to control film thickness and uniformity. The spin coater initiates, causing the substrate to rotate at the specified speed. This rotation spreads the solution radially, creating a thin film.

As the substrate rotates, the solvent in the solution evaporates, leaving behind a solid film. Upon completing the process, the film's quality and thickness can be inspected using appropriate characterization techniques.

2.1.2 Making the samples

First, an acid piranha solution, composed of sulfuric acid (H_2SO_4) and hydrogen peroxide (H_2O_2) in a 3:1 ratio, is prepared. This potent oxidation process eliminates organic impurities and simultaneously renders the substrate surface hydrophilic.

The substrates are immersed in this solution and left for one hour at 90°C . Subsequently, a basic piranha solution, made from ammonium hydroxide (NH_4OH) and hydrogen peroxide (H_2O_2) in a 3:1 ratio, is prepared.

After multiple cleanses in Milli-Q water (with a resistivity of 18.2 MΩ/cm at 25°C), the substrates are immersed for 20 minutes at 90°C. in this basic solution. Finally, the substrates are thoroughly washed and placed in Milli-Q water before use.

In our specific case, the substrate consists of silica glass (SiO2), which serves as the foundation for the thin film. The top part of the substrate has been coated with a layer of liquid Dimethyl sulfoxide (DMSO). This DMSO layer acts as a medium for the organic dye, specifically IR-140, which has been dissolved in it.

The spin coating process involves the following steps:

1. Dissolving the dye: Initially, the organic dye IR-140 is dissolved in the liquid DMSO. This solution is prepared to ensure that the dye is uniformly dispersed in the liquid.

2. Applying the solution: The prepared dye-DMSO solution is carefully deposited onto the top part of the silica glass substrate. It's essential to ensure an even and consistent coverage across the surface.

3. Centrifugation: The coated substrate is then placed on a spin coater, a specialized device designed for this purpose. The substrate is secured to a spinning chuck.

4. Spin Coating: The spin coater is activated, and the chuck starts to spin rapidly. As the substrate spins, centrifugal force causes the solution to spread outwards from the center of the substrate.

5. Thin Film Formation: During this process, the solvent (DMSO) rapidly evaporates due to the spinning motion and exposure to air. This results in the deposition of a thin and uniform film of the organic dye on the silica glass substrate. The thickness of the film can be controlled by adjusting the spin coating parameters such as spin speed, spin time, and the concentration of the dye solution.

6. Final Film: Once the spin coating process is complete, you are left with a thin film of IR-140 dye on the silica glass substrate. This film is characterized by its uniformity and thickness, making it suitable for various applications such as optical or electronic devices.

The selection of the substrate and the covering material was made with the aim of achieving a near-perfect match in refractive indices, as if the NP array were situated in a homogeneous medium. At a vacuum wavelength of 800 nm, silica exhibits a refractive index of approximately n_{SiO_2}, while the refractive index of DMSO is $n_{DMSO} = 1.476$ at 600 nm.

This process repeat agin with another substrate and solution with different concentration which I explain in the experimental working.

Chapter 3

Experimental

3.1 Gold Nanostructured Arrays

The initial sample used in this study consists of a square grid nanodisks of Au. These nanodisks were created using Electron Beam Lithography (EBL). The distance between each nanodisk in the lattice, denoted as p, is approximately 590 nanometers. The nanodisks themselves are shaped like cylinders, with a diameter (r) of 120 nanometers and a height (H) of 50 nanometers as shown in the Fig 3.1. The entire patterned surface spans a square region measuring $500\,\mu\text{m} \times 500\,\mu\text{m}$.

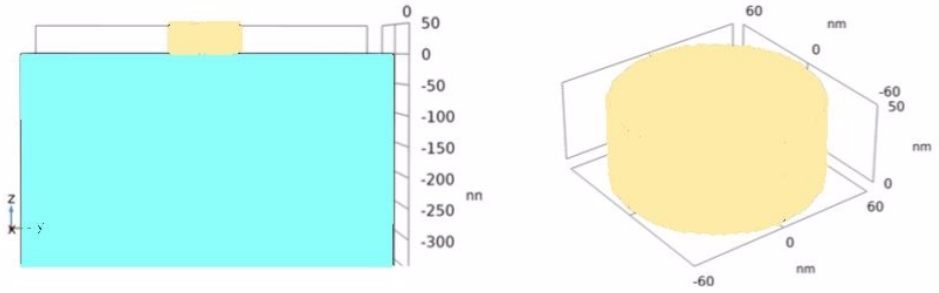

Figure 3.1: Gold nanoparticle

3.2 Morphological Characterization

We use Scanning Electron Microscopy (SEM) and Atomic Force Microscopy (AFM) to analyze the materials form and structure. Both techniques were utilized to estimate the lattice parameter and compare it to the expected value. Specifically, SEM provides high-magnification, high-resolution images, while AFM enables the estimation of the height of the gold nanodisks.

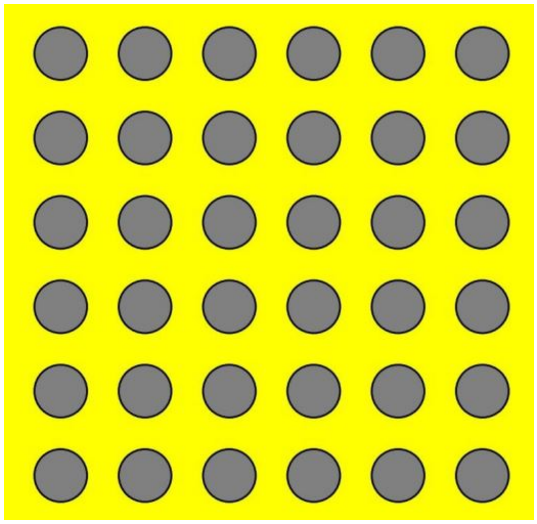

Figure 3.2: Gold nanoparticle in square array

3.2.1 Atomic Force Microscopy (AFM)

Atomic Force Microscopy (AFM) stands as a versatile and indispensable tool in the realm of nanoscience and material characterization. Operating on principles rooted in nanoscale interactions, AFM enables the high-resolution imaging and probing of surfaces with remarkable precision. This technique hinges on the interaction between a sharp probe tip and the sample surface which is in Fig 3.3, capturing the intricate details of atomic and molecular structures[19].

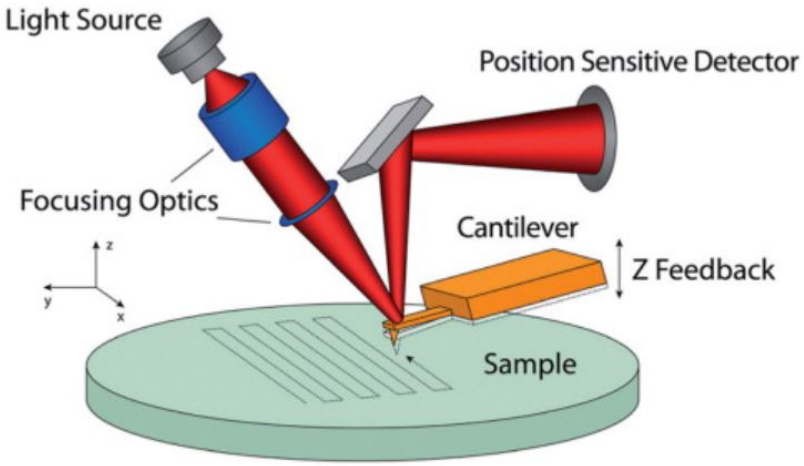

Figure 3.3: scheme of an AFM in tapping mode[20]

In its essence, AFM utilizes a cantilever and tiny, flexible beam typically made of silicon or silicon nitride with a sharp probe tip at one end. The key working principles revolve around the interaction forces that come into play when this tip approaches the sample. These forces encompass van der Waals forces, chemical bonding, and electrostatic forces[21].

The AFM process involves monitoring the reflection of a laser beam on the back of the cantilever. Any deflection or bending of the cantilever as it interacts with the sample surface is meticulously recorded by a position-sensitive photodetector. A continuous feedback loop ensures that the probe tip maintains a constant deflection, thereby generating a detailed topographical map of the sample surface.

AFM can be employed in various imaging modes, such as Contact Mode, semi-contact Mode, and Non-Contact Mode, as shown in Fig3.4, each offering distinct advantages depending on the specific research goals. Contact Mode involves continuous interaction between the tip and the sample, whereas semi-contact Mode gently taps the surface at its resonance frequency. In Non-Contact Mode, the tip hovers just above the surface without direct contact.

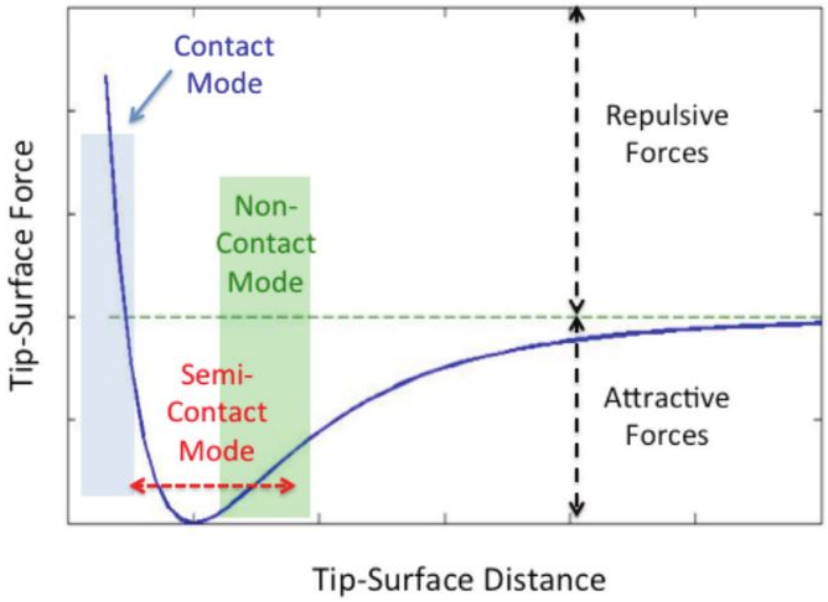

Figure 3.4: scheme of the working modes for an AFM

Contact Mode (AFM):

In Contact Mode AFM, the AFM tip continuously touches the sample surface. The tip is attached to a flexible cantilever, and as it scans across the sample, the cantilever deflects in response to forces between the tip and the sample, including van der Waals forces and electrostatic interactions. This mode is relatively simple to operate and provides high-resolution imaging. However, it carries the risk of damaging soft or delicate samples due to continuous physical contact and higher interaction forces.

Semi-contact Mode (AFM):

Semi-contact Mode AFM, also known as Intermittent Contact Mode, is an improvement over Contact Mode. Instead of constant contact, the tip lightly taps or oscillates near the sample surface. The cantilever's resonant frequency changes as the tip approaches the sample, and this change is used to create images. Semi-contact Mode reduces the risk of sample damage, provides excellent lateral resolution, and is suitable for delicate samples.

However, it requires precise control of the oscillation parameters and careful calibration.

Non-Contact Mode (AFM):

In Non-Contact Mode AFM, the tip hovers just above the sample surface without physical contact. It measures forces such as van der Waals forces while maintaining a non-contact position, typically a few nanometers above the surface. This mode minimizes sample interaction and is suitable for high-resolution imaging. Researchers select the mode that best suits their samples and research requirements based on the characteristics of their materials and the desired resolution. In this research, we opted for the semi-contact mode

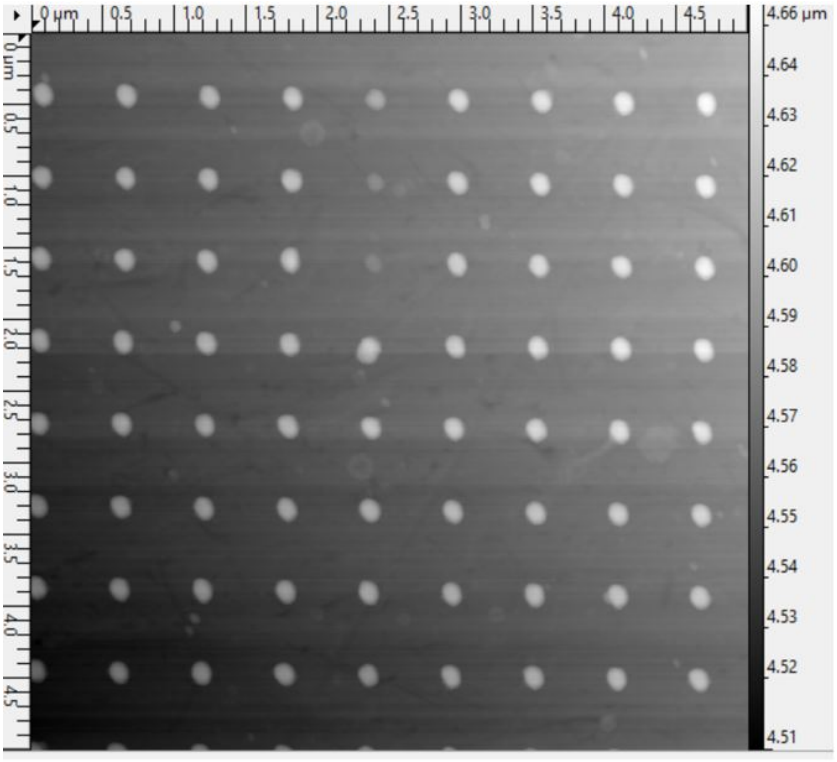

Figure 3.5: scan with a smaller area of the sample

instead of the full-contact mode to minimize the potential damage to the nanostructured arrays.

The AFM images were captured using the semi-contact mode, scanning a region measuring $10 \times 10\,\mu m^2$ on the $500 \times 500\,\mu m^2$ array. Subsequently, the obtained data was analyzed using the Gwyddion software.

3.2.2 Scanning Electron Microscopy(SEM)

Scanning Electron Microscopy (SEM) is a powerful imaging technique used extensively in scientific research and industrial applications. It enables the detailed analysis of microstructures and surface topography of various materials. SEM is particularly providing crucial insights into the morphology of specimens.

The operating principle of SEM involves scanning a focused electron beam across the

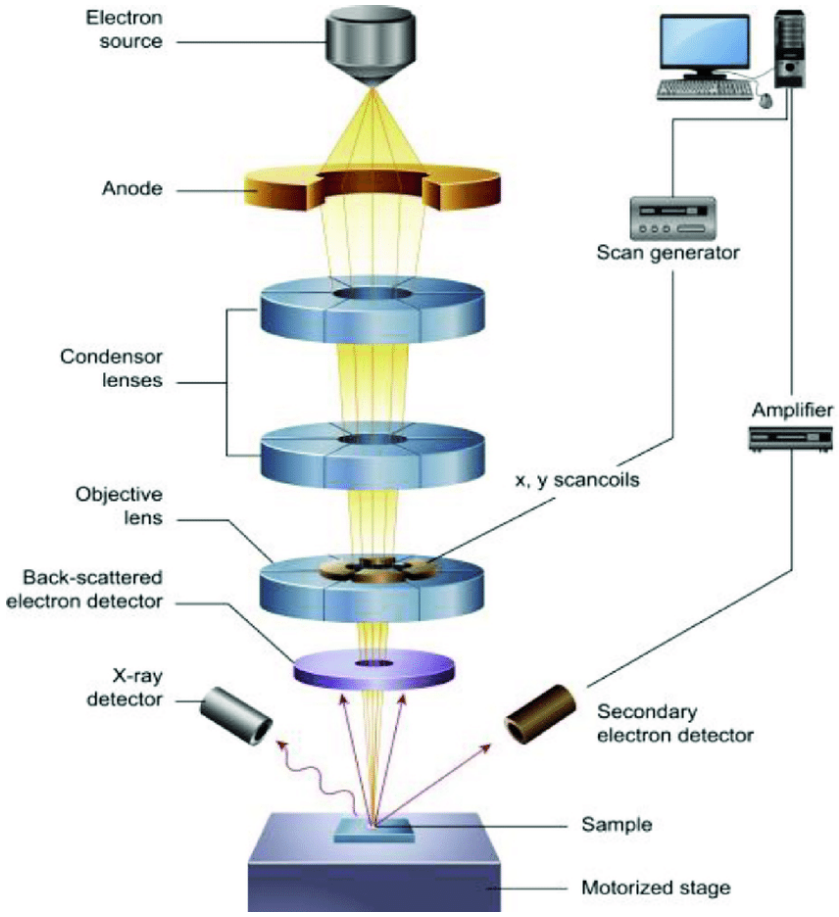

Figure 3.6: scheme of a SEM

surface of the sample. As the electrons interact with the sample, they generate various signals, including secondary electrons and backscattered electrons as shown in Fig 3.6. These emitted electrons are detected and utilized to create images. Secondary electrons offer high-resolution surface topography details, while backscattered electrons convey information about the sample's atomic composition.

One key factor in SEM is the depth of electron penetration (d), which quantifies the distance electrons penetrate into the sample:

$$d = \frac{4}{3}\frac{\rho}{\rho_e}\frac{Z}{\mu}\frac{E_0}{\Delta E}$$

Here, d represents the depth of electron penetration, ρ is the sample density, ρ_e is the electron density, Z is the atomic number, μ is the mean energy loss per unit length, E_0 is the initial electron energy, and ΔE is the energy loss. This equation provides insights into how electrons interact with the sample, influencing SEM image formation.

The equipment employed in this study is an FE-SEM (Zeiss Sigma HD). To serve our specific objectives, we applied a 5 kV electron beam and detected backscattered electrons, as our primary concern was the material contrast within the array. Opting for a lower energy beam was primarily to prevent surface charging, particularly due to the dielectric

substrate's presence.

3.2.3 SEM images

The sample was also examined with the Scanning Electron Microscope (SEM) by collecting backscattered electrons. The resulting image is shown in Figure and analyzed with Images. Two lines, 1 and 2 in Fig 3.7, were drawn, and the intensity profile along both of them has been analyzed.

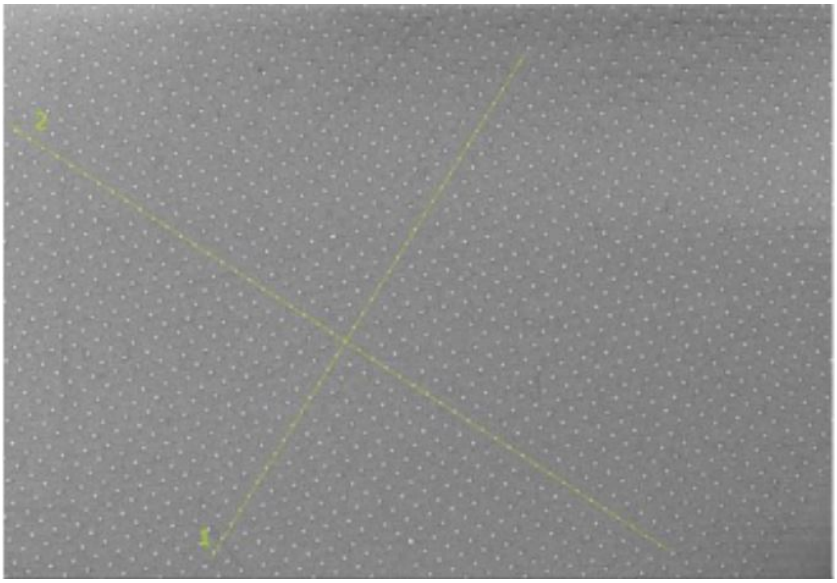

Figure 3.7: SEM image of the sample

The result of this analysis is as follows: $a_1 = (602)$ nm and $a_2 = (598)$ nm, which are compatible with both the AFM estimates and the nominal value.

The average value of lattice constant is around 600 nm and the height of the sample measured 50 nm.

3.3 Lasing Emission Setup

A pulsed laser beam undergoes attenuation using switchable optical density filters before being directed towards the sample under examination with the aid of reflective mirrors. The sample is fixed on the rotating arm, providing control over the angle of incidence. Additionally, a lens can be incorporated into the beam path to focus the beam and alter its radius in the sample plane. The collection system comprises a rail that can pivot around the sample, and the HR4000 Ocean Optics spectrometer is positioned at a designated distance from the sample.

By rotating the rail, it becomes possible to gather wavelength spectra at varying emission angles and construct an emission map. Conversely, by adjusting the optical density (OD) filters, one can investigate the output power relative to the input power and generate a graph illustrating the pump threshold.

Mounted on the rail are several devices, including a long-pass filter designed to eliminate any remaining pump light, a collimator lens, and the end of an optical fiber connected to the spectrometer. The specifics of the laser beam and various optical components (such as mirrors and filters) as shown in Fig 3.8 are adjusted according to the sample and the specific measurements being conducted.

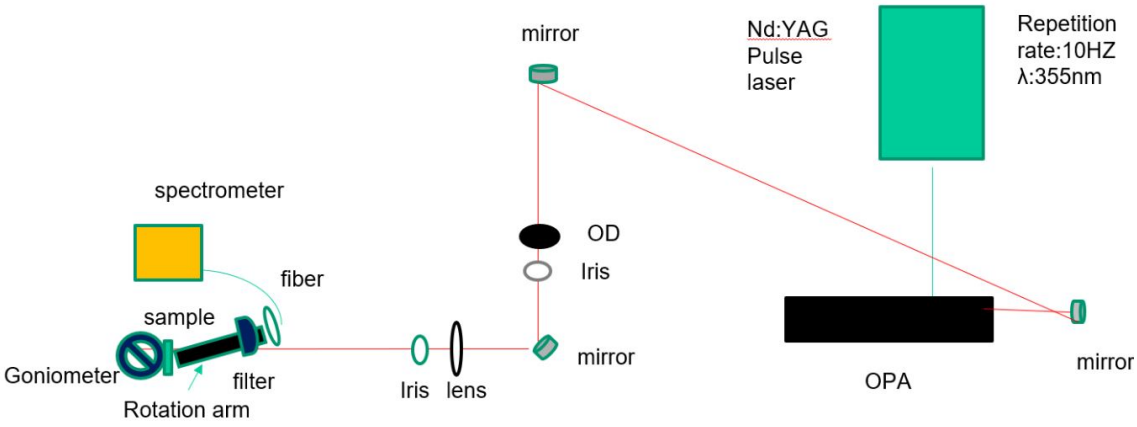

Figure 3.8: Scheme of the setup for measurement of the lasing emission of the sample

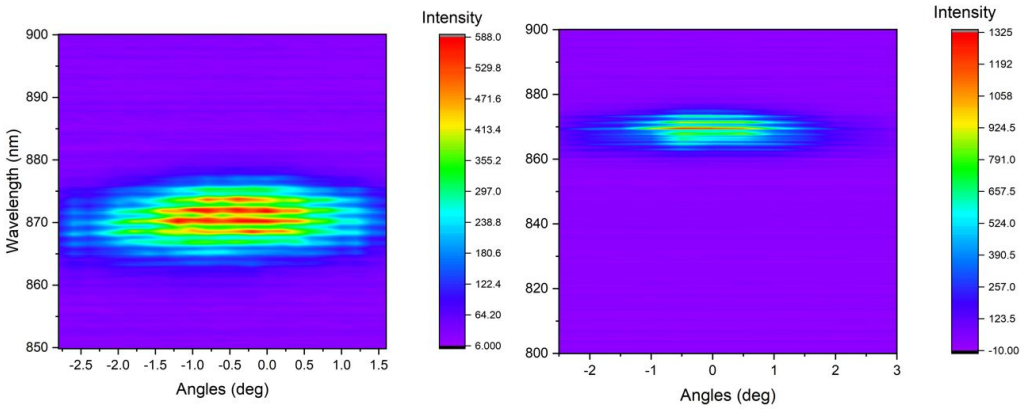

Figure 3.9: Left:fluorescence map take with the setup, Right:Emission map of the Au square sample with the setup

In addition to generating emission maps and determining the lasing threshold, this configuration can also be utilized for obtaining polarization maps as we can see in Fig3.9. The process is straightforward: the system is excited with a constant power exceeding the lasing threshold, and light is collected in the direction of emission. A polarizer filter is then inserted into the rotating rail, just before the emitted light enters the collimator lens. By systematically adjusting the polarizer filter over the entire 0° to 360° range and recording the emission peak height as a function of the polarizing angle θ, one can create a comprehensive polarization map of the lasing light.

this results are for the liquid matrix, and now we want to study in the solid matrix.Solid

matrices are often more stable and have longer lifetimes compared to liquid matrices. They are less prone to degradation over time due to environmental factors or chemical reactions.This stability can help reduce photobleaching, which is the phenomenon where dye molecules lose their ability to absorb and emit light after prolonged exposure.

3.4 Characterization of the emitter

To assess the optical characteristics of the emitter, a dye IR-140 was formulated. Subsequently, absorbance and emission spectra were recorded using various instruments.

3.4.1 Absorbance measurments

The Jasco V-670 spectrophotometer is a high-performance, double-beam UV-Vis-NIR (Ultraviolet-Visible-Near Infrared) spectrophotometer manufactured by JASCO Corporation as shown in Fig 3.10. It is designed to measure the absorption of light in a wide spectral range, from the ultraviolet (UV) to the near-infrared (NIR) regions, providing us with valuable data about the optical properties of samples.

Figure 3.10: photo of the Jasco V-670 spectrophotometer

The instrument operates on the principle that different substances absorb light at different wavelengths, allowing us to quantitatively analyze the concentration and optical properties of substances. It consists of various components as we can see the scematic in Fig 3.10, including a light source, a monochromator, a sample holder, and a detector. The instrument typically uses a deuterium lamp for the UV range and a halogen lamp for the visible and NIR range as its light sources. These lamps emit light over a broad spectrum of wavelengths.

The monochromator is responsible for selecting specific wavelengths of light and directing them towards the sample. It does so by dispersing the incoming white light into its

constituent colors (spectrum) and then isolating the desired wavelength. Samples can be loaded into the instrument's sample holder, and their absorption is measured at different wavelengths.

The sample holder is designed to accommodate a variety of sample types, such as liquids, solids, and gases. The Jasco V-670 employs a photomultiplier tube (PMT) or other suitable detectors to measure the intensity of light that passes through the sample at each wavelength.

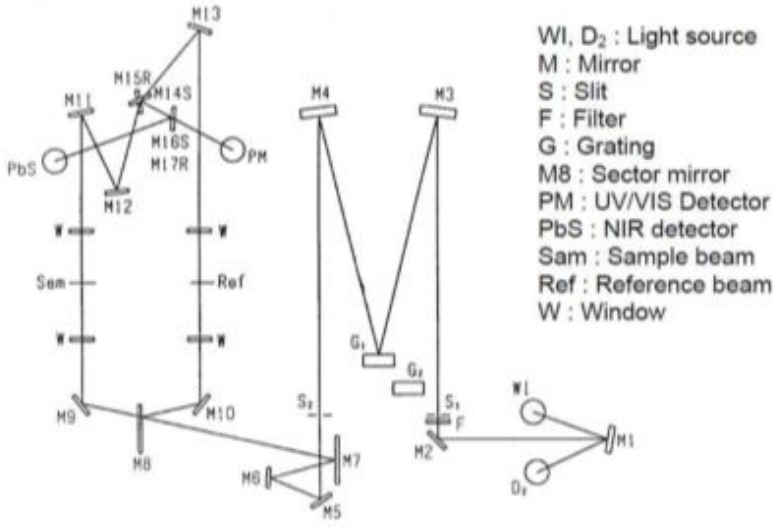

Figure 3.11: scheme of a Jasco V-670

Absorbance is linearly related to the distance, denoted as 'z,' over which light passes through the sample. Specifically, within a liquid solution, light intensity experiences attenuation along its propagation path. This phenomenon is described by the formula:

$$I(z) = I_0 e^{-\gamma z} \tag{3.1}$$

where γ represents the extinction coefficient.

Absorbance can be defined :

$$A = \log_{10} \frac{1}{T} = \gamma z \log_{10} e \tag{3.2}$$

, where 'z' represents the coordinate along the 'z' axis, 'T' is the transmittance

$$T = \frac{I}{I_0} \tag{3.3}$$

, and 'e' is the base of the natural logarithm.

3.4.2 Fluorescence measurments

Fluorescence spectrum refers to the emission of light (fluorescence) by a substance when it absorbs photons of a shorter wavelength and then re-emits them at longer wavelengths. This phenomenon is commonly used for analyzing the optical properties of various materials, including molecules, nanoparticles, and biological samples.

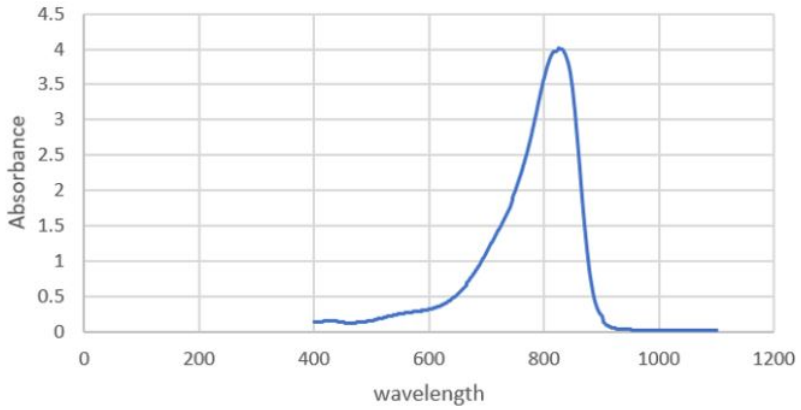

Figure 3.12: Absorbance spectrum of dye IR140

The Fluoromax as shown in Fig 3.13 is a type of fluorescence spectrometer used for recording fluorescence spectra.

Figure 3.13: image of the spectrofluorometer

Fluorescence spectrometers like the Fluoromax typically consist of several key components which shown in Fig 3.15, including a light source (usually a xenon or mercury lamp), monochromators to select specific excitation and emission wavelengths, a sample chamber, and a detector (photomultiplier tube or CCD detector) to measure the emitted fluorescence.

Fluorescence spectrometers like the Fluoromax provide data in the form of fluorescence spectra. These spectra display the intensity of emitted light (fluorescence) as a function of wavelength.

The formula for fluorescence emission can be given by the following equation:

$$F(\lambda) = \varepsilon(\lambda) \cdot C \cdot \Phi \cdot I(\lambda)$$

Where $F(\lambda)$ represents the fluorescence emission intensity at a particular wavelength λ, $\varepsilon(\lambda)$ is the molar absorptivity (extinction coefficient) of the fluorophore at wavelength λ, C

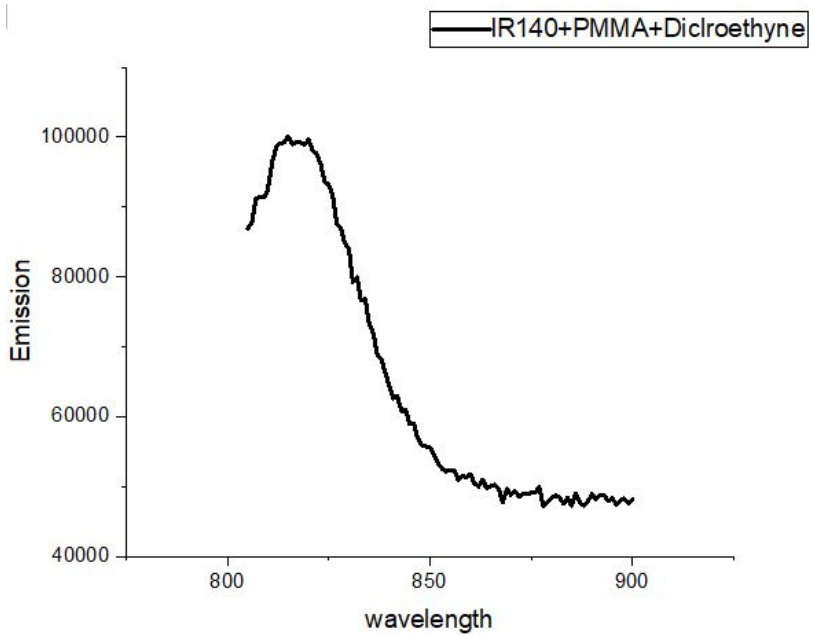

Figure 3.14: Emission plot IR140 with PMMA and Dicloroethyne

is the concentration of the fluorophore,Φ is the quantum yield, representing the efficiency of fluorescence emission and $I(\lambda)$ is the intensity of the incident light at wavelength λ.

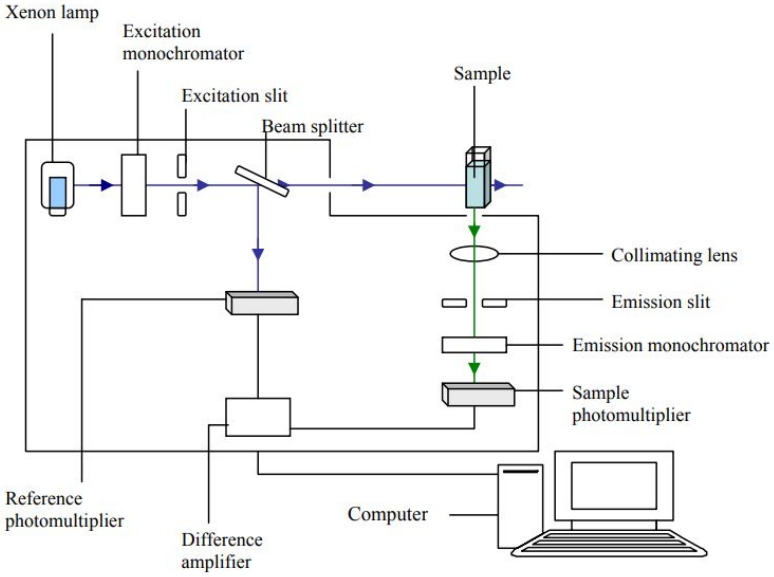

Figure 3.15: schematic of the fluoromax

Chapter 4

Results and Discussion

In this chapter we will present the main results obtained in this thesis. First of all the most relevant results regarding the active medium and the nanostructured material will be discussed. Then we will go into the main topic of this work, i.e., the changing of the concentration of dye and focus on absorbance and emission.

4.1 Dye-doped polymer film

4.1.1 Sample prepration

Some different solutions were prepared by dissolving 100 mg of PMMA in 1 ml dichloromethane and adding IR-140 to PMMA with a weight ratio of 1wt percent, 2wt percent and 5 wt percent. After that we prepare of glass substrates and the concentration of PMMA is 2%, the corresponding IR-140 concentration in the polymer is then 2%, 3% and 5% , respectively. Solutions were then spin-coated on clean standard microscope glass slides, for 50 second at 3000 rpm, 2500rpm, 2000rpm and 1500rpm and baked at 30°C for 10 minutes.

4.1.2 Thickness measurement with AFM

In this study, we investigate a doped layer on a silicon substrate, which comprises 1% dye IR140 as a gain medium and varying concentrations of PMMA, including 1%, 2%, and 5%. These layers are dissolved in a dichloroethane solvent. The results of the thickness in Fig 4.1, we prepared the three sample with 1500 rpm, 2500rpm and 3000rpm. As we can see in the figure 4.1 the thickness for IR140(1%), PMMA(1%) is between 55nm to 75nm, for IR140(1%), PMMA(2%) is around 150nm to 170nm and for the IR140(1%), PMMA(5%) is 400nm to 600nm.

Then we used the glass substrate and choose the best samples with more homogeneity and without the defects with 2% PMMA and we the change the consentration of dye to 1% , 2% and 5%, and we set the 1500rpm , as we can see in the Fig 4.2. For IR140(1%), PMMA(2%) the thickness is around 70nm, for IR140(3%), PMMA(2%) is around 170nm and for the IR140(5%), PMMA(2%) is around 500nm.

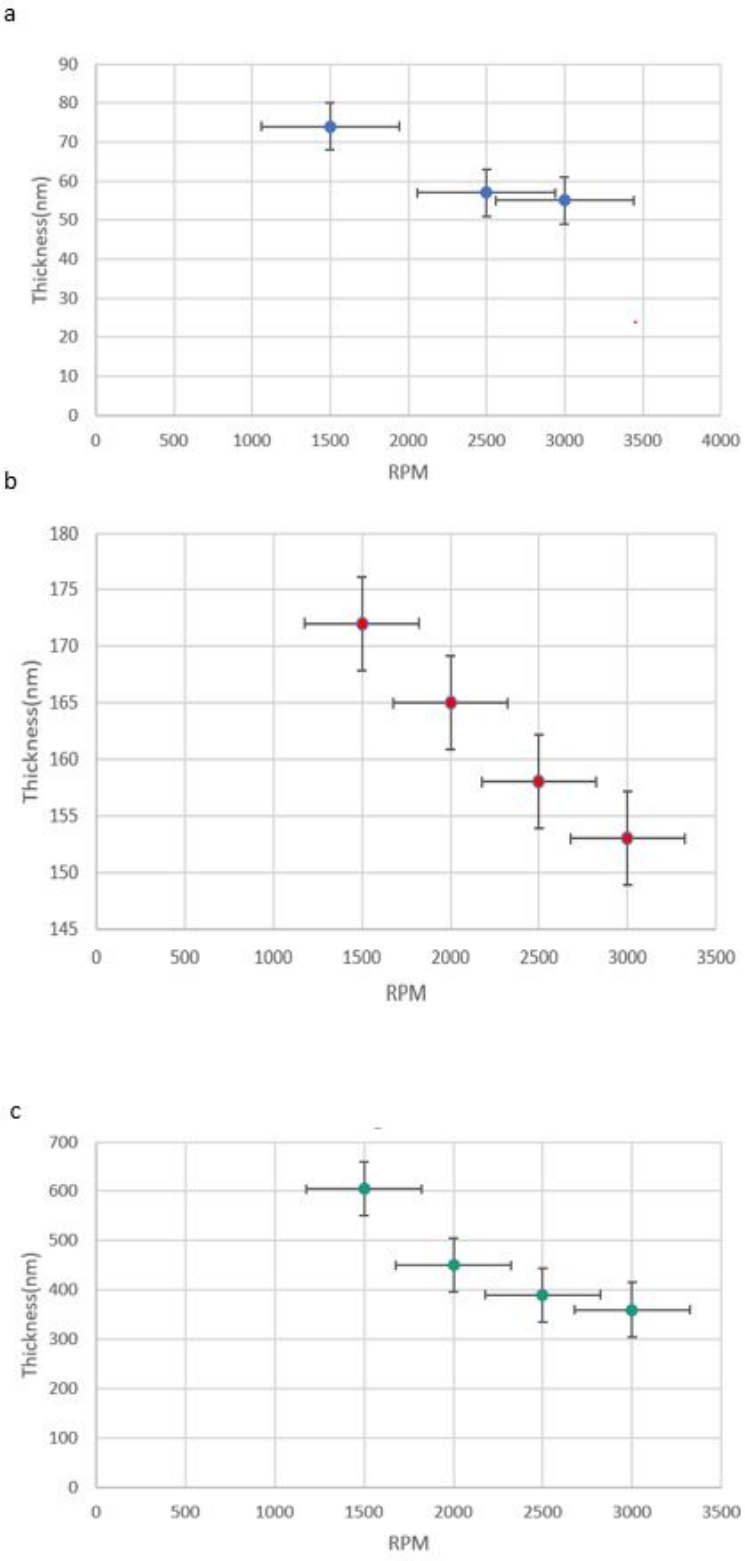

Figure 4.1: Thickness plots of silicon with (a) IR140(1%), PMMA(1%), (b) IR140(1%), PMMA(2%) and (c) IR140(1%), PMMA(5%) and Diclroethyne spinnedf at different rpm

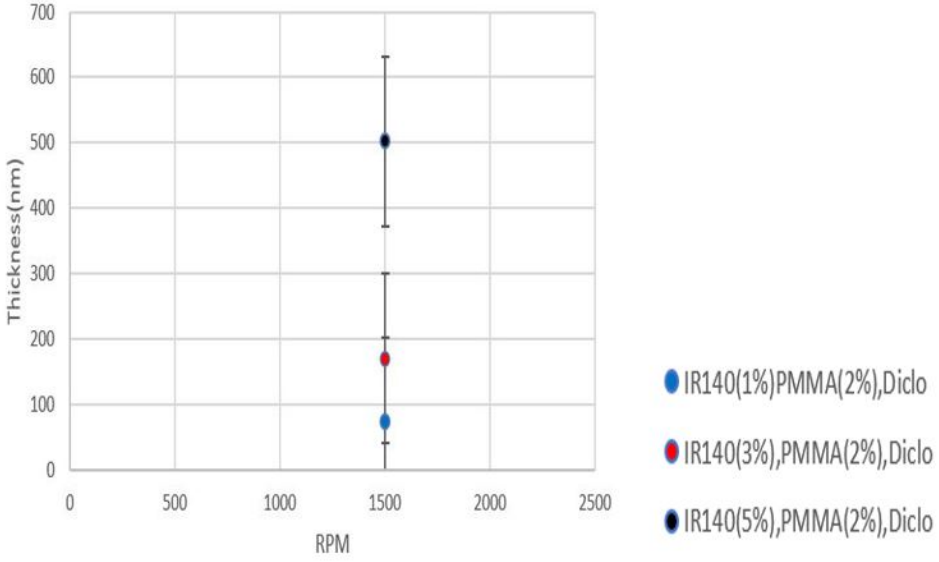

Figure 4.2: Thickness plots of glass with different concentration of dye IR140 and the 2% of PMMA and Dicloroethyne with fixed 1500 rpm

4.2 Absorbance measurement of the dye-doped

The principal aim of this part is to explore the absorbance characteristics of layers doped with 1% dye IR140 and varying concentrations of PMMA (1%, 2%, and 5%) in dicloroethyne. These measurements are of profound significance as they shed light on the interaction of diverse materials and the influence of different PMMA concentrations on their optical properties. The spectrophotometer was meticulously configured with specific settings, including a glass baseline, a 2 nm band width, a scanning speed of 400 nm/min, and a wavelength range spanning from 450 nm to 1100 nm. The prepared samples, consisting of the glass substrate and doped layers, were placed in the spectrophotometer's sample holder, and the absorbance measurements were executed. This comprehensive analysis aims to elucidate the absorption characteristics at distinct wavelengths and the repercussions of varying PMMA concentrations on the absorbance spectra.

The absorbance spectra derived from these measurements are slated for thorough examination to uncover the absorption properties of the silicon substrates doped with 1% dye IR140 and varying concentrations of PMMA (1%, 2%, and 5%). This analytical endeavor will unravel the intricacies of the optical behavior of these materials, delineating their absorption peaks and, more notably, delineating the influence of PMMA concentration on their absorbance. We can see the results in Figure 4.3. A well-defined peak can be identified and its maximum corresponds to a wavelength of 820 nm.

Then we prepared another samples set with different concentration of dye (1%, 3%, and 5%) and 2% PMMA in the solvent dicloroethyne. The results shown in the Figure 4.4. When the concentration of a dye in a solution is changed while keeping other factors, including solvent and polymer, the absorbance of the solution can exhibit a proportional

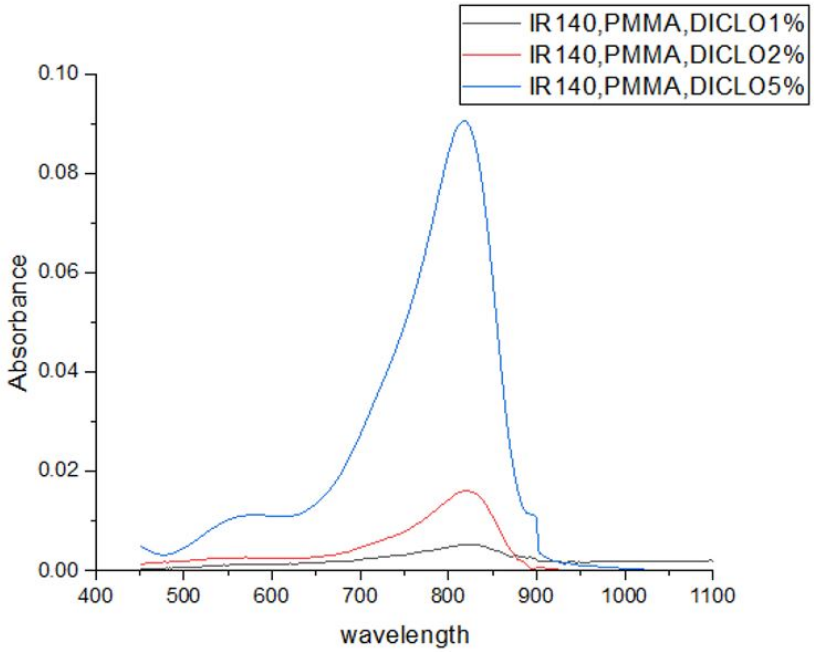

Figure 4.3: Absorbance plots of layers with 1% IR140 and varying concentrations of PMMA (1%, 2%, and 5%) and Dicloroethyne

relationship to the concentration of the dye. If we change the concentration of the dye, we should observe a linear relationship between the absorbance and the dye concentration. As the concentration of the dye increases, the absorbance should also increase proportionally.

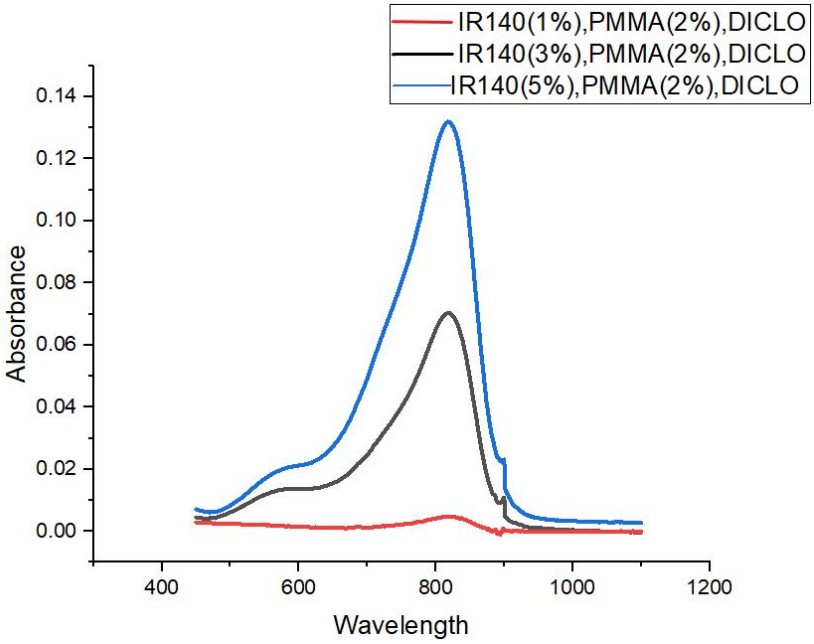

Figure 4.4: Absorbance plots of layers with 2% PMMA and varying concentrations of IR140 (1%, 3%, and 5%) and Dicloroethyne

4.3 Emission Measurement with Fluoromax

In our endeavor to reveal the emission characteristics of our samples, we utilized the capabilities of the Fluoromax fluorescence spectrometer, configuring it to its optimal parameters. The spectroscopic exploration initiated with an initial wavelength of 805 nm and concluded at 900 nm, facilitating the capture of emission spectra across a significant range for a detailed examination of the fluorescence properties of the materials. To ensure measurement precision, the integration time was carefully set to 2 seconds, enabling accurate capture and recording of the emitted fluorescence.

The excitation source employed a wavelength of 800 nm, effectively stimulating the samples and initiating fluorescence emission. This process was further refined by selecting excitation and emission wavelengths with slit widths of 3 nm and 5 nm, respectively, providing us with the ability to precisely control the spectral parameters. These meticulous experimental conditions were designed to reveal the detailed fluorescence characteristics of the samples, providing valuable insights into how PMMA concentration influences fluorescence spectra and the interactions between these materials and their surrounding environment.The results are shown in Fig 4.5.

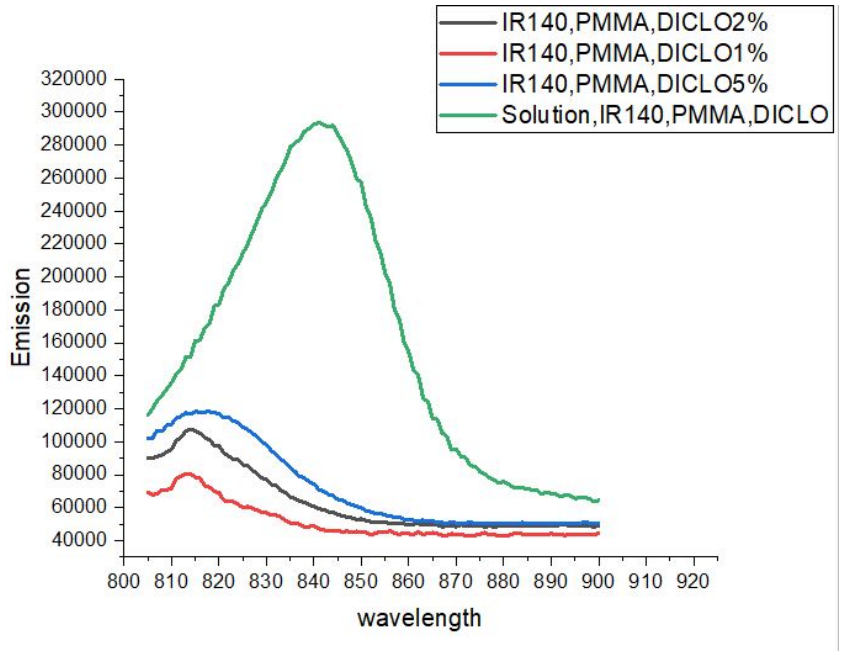

Figure 4.5: Emission plots of layers with 1% IR140 and varying concentrations of PMMA (1%, 2%, and 5%) and Diclroethyne and the emission of the solution

It was observed that an increase in the concentration of PMMA led to a progressive enhancement in the intensity of the emitted fluorescence. The thickness of the layers for 1% PMMA is 70 nm, 2% PMMA is 170nm and 5% PMMA 500nm.

More specifically, the fluorescence intensity exhibited a proportional relationship with the concentration of PMMA, indicating that higher PMMA concentrations resulted in stronger fluorescence emissions.

The emission measurements illuminated a discernible pattern in the fluorescence behavior of the samples when the concentration of IR140 dye was altered. Notably, an increase in the concentration of IR140 dye led to a consistent and incremental amplification in the intensity of the emitted fluorescence.

The optical properties of the Au square array were investigated using a finite-element method, which involves solving the problem on a discretized grid. The simulation was conducted with COMSOL Multiphysics.

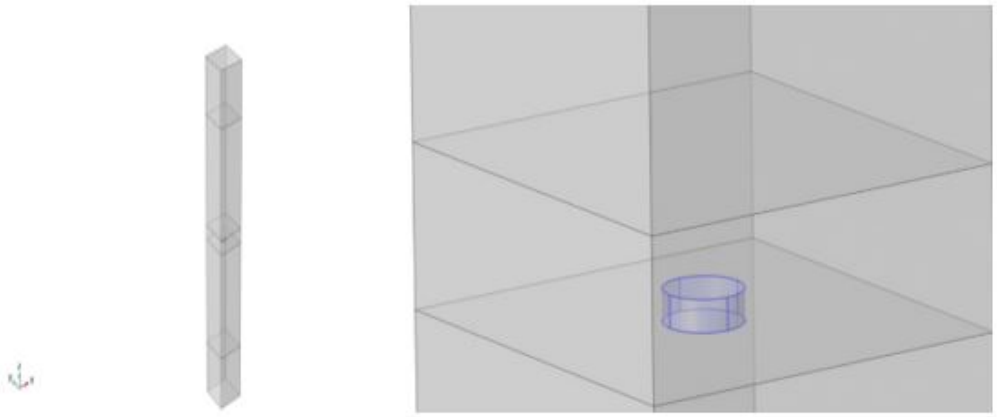

Figure 4.6: Three-dimensional depictions of the fundamental unit employed in the COMSOL simulation

From a geometric perspective, our simulation domain is defined as a square primitive cell with a square base measuring 600×600 nm^2. Within this cell, the top and bottom regions extending 250 nm serve as perfectly matched layers (PMLs). These PMLs essentially function as high-absorption layers, designed to dampen radiation at the vertical edges of the cell and prevent any potential reflections along the vertical edges during the calculations.

In Fig 4.6, shown the unit cell emploied for comsol simulation. The substrate, a fundamental component, is comprised of silica glass. It was modeled as a dielectric layer with a well-defined height of 600 nm and exhibited a constant refractive index of 1.54. This detailed modeling allowed us to accurately capture the optical behavior of the silica layer and its interactions with incident light.

Furthermore, the upper portion of the structure, which is constructed from PMMA (Poly(methyl methacrylate)), shares the same height of 600 nm but possesses a distinct refractive index of 1.46. The presence of PMMA introduced a unique optical characteristic to the system, and its accurate representation was crucial in our simulation.

Within this PMMA layer, we strategically positioned a Gold cylinder, which made direct contact with the underlying silica layer.

4.3.1 Thickness analysis

The graph 4.7 which is provided be a plot of extinction versus wavelength for different thicknesses of PMMA (polymethyl methacrylate) layers doped with the dye IR140, placed on a glass substrate, and with dichloroethane as the solvent.

Lasing emission occurs when the energy absorbed by the dye molecules is released in the form of light. The peaks in the extinction curve correspond to the wavelengths at which lasing emission is most efficient.

The extinction peaks vary with the thickness of the PMMA layers, indicating that the optical properties of the dye-doped PMMA are thickness-dependent.

On the other hand,the sharp peaks, especially noticeable at higher wavelengths (near the 870 nm), are likely the wavelengths where lasing emission occurs. These peaks are more pronounced at certain thicknesses (e.g., 200 nm and 400 nm), which could mean that these thicknesses are more favorable for lasing due to the constructive interference and the resonant cavity effect created by the layer thickness. we choose the 200 nm because the sample was more homogeneous. The peak intensity and position change with the layer thickness, which suggests that the optical feedback within the PMMA layers is affected by the thickness.

Dicloroethyne as the solvent may have an effect on the dissolution and dispersion of the IR140 dye within the PMMA, which in turn could influence the extinction properties and the efficiency of the lasing emission. The use of a glass substrate can also affect the lasing characteristics since it can act as part of the optical cavity, influencing the feedback mechanism of the emitted light.

In conclusion, the most significant lasing emissions appear to be in the near-infrared region, just beyond 870 nm, which is consistent with the known absorption/emission properties of IR140 dye. The exact position and intensity of these emissions vary with the thickness of the PMMA layers, which could be due to the variations in optical path length and interference effects within the layers.

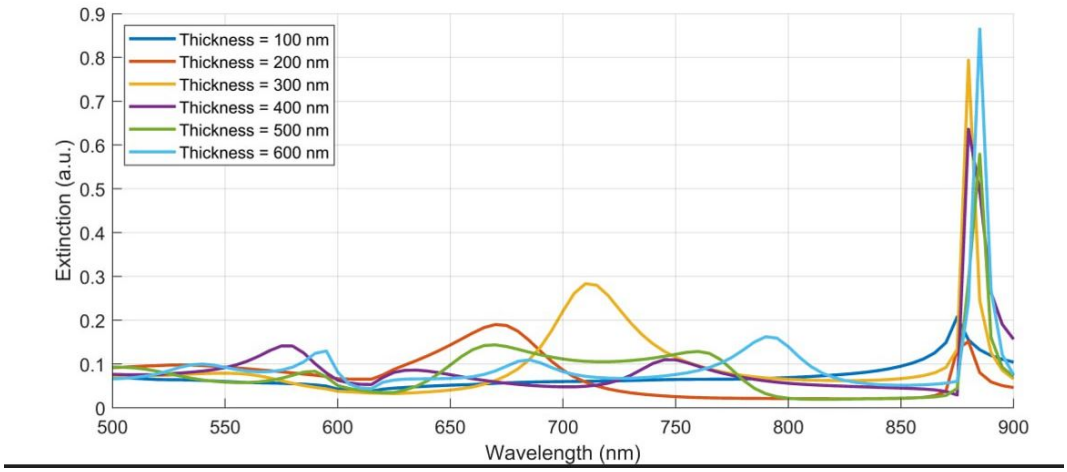

Figure 4.7: Simulated the lasing emission peaks with different thicknesses of thr dye-doped PMMA

Chapter 5

Conclusions

The aim of this work was the synthesis and characterization of dye-doped polymeric thin films.

In this study, we examine the dye-doped layers, comprising 1% dye IR140 as and varying concentrations of PMMA (1%, 2%, and 5%).Three samples were prepared using spin speeds of 1500 rpm, 2500 rpm, and 3000 rpm. The thickness for IR140(1%) and PMMA(1%) falls between 55 nm and 75 nm, while for IR140(1%) and PMMA(2%), it ranges from 150 nm to 170 nm. For IR140(1%) and PMMA(5%), the thickness is approximately 400 nm to 600 nm. We choose the sample with PMMA(2%) because it was more homogeneous and without the defects. We adjusted the dye concentration to 1%, 2%, and 5%, maintaining a spin speed of 1500 rpm. For IR140(1%) and PMMA(2%), the thickness was approximately 70 nm. In the case of IR140(3%) and PMMA(2%), the thickness reached around 170 nm, while for IR140(5%) and PMMA(2%), the thickness was approximately 500 nm.

Then we measured the absorbance of the doped layers doped with 1% dye IR140 and varying concentrations of PMMA (1%, 2%, and 5%). This analysis aims to unveil the optical properties, including absorption peaks, and importantly, the impact of PMMA concentration on absorbance. A distinct peak is observed with its maximum at a wavelength of 820 nm.Then we prepared samples with different concentration of dye (1%, 3%, and 5%) and 2% PMMA in the solvent dicloroethyne.

Finite-element simulations were performed on the Au square array, in order to study the efficient of the different thickness of the layers to compare with the experimental methods. The prominent lasing peak, at 875 nm is pronounced at a thickness of 200 nm , suggesting that this thickness value is more favorable for lasing, possibly due to constructive interference and the resonant cavity effect.

Bibliography

[1] Jae Yong Suh, Chul Hoon Kim, Wei Zhou, Mark D. Huntington, Dick T. Co, Michael R. Wasielewski, and Teri W. Odom. Plasmonic bowtie nanolaser arrays. *Nano Letters*, 12(11):5769–5774, 2012.

[2] Wei Zhou, Montacer Dridi, Jae Yong Suh, Chul Hoon Kim, Dick T. Co, Michael R. Wasielewski, George C. Schatz, and Teri W. Odom. Lasing action in strongly coupled plasmonic nanocavity arrays. *Nature Nanotechnology*, 8(7):506–511, 2013.

[3] Ankun Yang, Thang B. Hoang, Montacer Dridi, Claire Deeb, Maiken H. Mikkelsen, George C. Schatz, and Teri W. Odom. Real-time tunable lasing from plasmonic nanocavity arrays. *Nature Communications*, 2015.

[4] Hsin-Yu Wu, Longju Liu, Meng Lu, and Brian T. Cunningham. Lasing emission from plasmonic nanodome arrays. *Advanced Optical Materials*, 2016.

[5] A. Hinke Schokker and A. Femius Koenderink. Lasing in quasi-periodic and aperiodic plasmon lattices. *Optica*, 3(7):686–693, 2016.

[6] Ren-Min Ma and Rupert F. Oulton. Applications of nanolasers. *Nature Nanotechnology*, 14(1):12–22, January 2019.

[7] Stefan A. Mayer. *Plasmonics: Fundamentals and Applications*. Springer, 2007.

[8] Gordon Gould. The laser, light amplification by stimulated emission of radiation. 15:128, 1959.

[9] E. Hecht. *Optics*. Pearson Education, 2002.

[10] Uwe Kreibig and Michael Vollmer. *Optical Properties of Metal Clusters*, volume 25. Springer Science & Business Media, 2013. 19.

[11] David Bergman and Mark Stockman. Surface plasmon amplification by stimulated emission of radiation: Quantum generation of coherent surface plasmons in nanosystems. *Physical Review Letters*, 90:027402, Feb 2003.

[12] Wei Zhou et al. Lasing action in strongly coupled plasmonic nanocavity arrays. *Nature Nanotechnology*, 8(7):506–511, July 2013.

[13] John Smith and Mary Johnson. Plasmon nanocavity array lasers: Cooperating over losses and competing for gain. *Journal of Plasmonics*, 15(3):245–262, 2020.

[14] P. B. Johnson and R. W. Christy. Optical constants of the noble metals. *Phys. Rev. B*, 6:4370–4379, Dec 1972.

[15] Sebastian Wuestner, Andreas Pusch, Kosmas L. Tsakmakidis, Joachim M. Hamm, and Ortwin Hess. Gain and plasmon dynamics in active negative-index metamaterials. *Philosophical Transactions of the Royal Society A: Mathematical, Physical and Engineering Sciences*, 369(1950):3525–3550, 2011.

[16] Montacer Dridi and George C. Schatz. Model for describing plasmon-enhanced lasers that combines rate equations with finite-difference time-domain. *JOSA B*, 30(11):2791–2797, 2013.

[17] R. M. Almeida, J. R. Berenguer, and A. J. F. Carvalho. Dip coating of organic-inorganic hybrid films. *Journal of Sol-Gel Science and Technology*, 2007.

[18] C. Y. Lin, K. C. Liu, and C. C. Lee. Spin-coating of thin and uniform polymer films. *Journal of Chemical Education*, 2002.

[19] G. Binnig, C. F. Quate, and Ch. Gerber. Atomic force microscope. *Phys. Rev. Lett.*, 56(9):930–933, 1986.

[20] Franz J. Giessibl. Advances in atomic force microscopy. *Rev. Mod. Phys.*, 75(3):949–983, 2003.

[21] Murugan Veerapandian and Kyusik Yun. Study of atomic force microscopy in pharmaceutical and biopharmaceutical interactions - a mini review. *Current Pharmaceutical Analysis*, 5:256–268, Aug. 2009.

List of Figures

1.1 Laser cavity composed of a gain medium between two reflective mirrors . . 3
1.2 Energy diagram illustrating how absorption, stimulated emission, and spontaneous emission work. 4
1.3 Three-level and four-level laser schemes 5
1.4 A diagram showing the collective oscillation of electrons in a metal under electric field 9
1.5 periodic nanoscale structure on surface 9
1.6 Triangular lattice in real space(left) and Reciprocal lattice(right) 10
1.7 Schematic illustration of a plasmonic nanolaser 11
1.8 Four-level model used to describe the dye molecule 13

2.1 Spin coating process.(a)polymer solution add to the substrate on the rotating platform.(b)evaporation process and liquid flow goes outward due to the centrifugal force.(c)angular velocity in different steps and times.(d)final polymer film. 16

3.1 Gold nanoparticle 19
3.2 Gold nanoparticle in square array 20
3.3 scheme of an AFM in tapping mode[20] 20
3.4 scheme of the working modes for an AFM 21
3.5 scan with a smaller area of the sample 22
3.6 scheme of a SEM 23
3.7 SEM image of the sample 24
3.8 Scheme of the setup for measurement of the lasing emission of the sample . 25
3.9 Left:fluorescence map take with the setup, Right:Emission map of the Au square sample with the setup 25
3.10 photo of the Jasco V-670 spectrophotometer 26
3.11 scheme of a Jasco V-670 27
3.12 Absorbance spectrum of dye IR140 28
3.13 image of the spectrofluorometer 28
3.14 Emission plot IR140 with PMMA and Dicloroethyne 29
3.15 schematic of the fluoromax 29

4.1 Thickness plots of silicon with (a) IR140(1%), PMMA(1%), (b) IR140(1%), PMMA(2%) and (c) IR140(1%), PMMA(5%) and Diclroethyne spinnedf at different rpm 32
4.2 Thickness plots of glass with different concentration of dye IR140 and the 2% of PMMA and Dicloroethyne with fixed 1500 rpm 33
4.3 Absorbance plots of layers with 1% IR140 and varying concentrations of PMMA (1%, 2%, and 5%) and Dicloroethyne 34
4.4 Absorbance plots of layers with 2% PMMA and varying concentrations of IR140 (1%, 3%, and 5%) and Dicloroethyne 34
4.5 Emission plots of layers with 1% IR140 and varying concentrations of PMMA (1%, 2%, and 5%) and Diclroethyne and the emission of the solution 35
4.6 Three-dimensional depictions of the fundamental unit employed in the COMSOL simulation 36
4.7 Simulated the lasing emission peaks with different thicknesses of thr dye-doped PMMA 38